



Universiteit
Leiden
The Netherlands

The stellar mass-size evolution of galaxies from $z=7$ to $z=0$

Mosleh, M.

Citation

Mosleh, M. (2013, June 12). *The stellar mass-size evolution of galaxies from $z=7$ to $z=0$* . Uitgeverij BOXPress : 's-Hertogenbosch. Retrieved from <https://hdl.handle.net/1887/20961>

Version: Corrected Publisher's Version

License: [Licence agreement concerning inclusion of doctoral thesis in the Institutional Repository of the University of Leiden](#)

Downloaded from: <https://hdl.handle.net/1887/20961>

Note: To cite this publication please use the final published version (if applicable).

Cover Page



Universiteit Leiden




The handle <http://hdl.handle.net/1887/20961> holds various files of this Leiden University dissertation.

Author: Mosleh, Moein

Title: The stellar mass-size evolution of galaxies from $z=7$ to $z=0$

Issue Date: 2013-06-12



The Evolution of the Mass-Size
Relation to $z = 3.5$ for UV-Bright
Galaxies and Submillimeter Galaxies
in the GOODS-NORTH Field

Moein Mosleh, Rik J. Williams, Marijn Franx, Mariska Kriek
The Astrophysical Journal, 2011, 727:5

Abstract

We study the evolution of the size-stellar mass relation for a large spectroscopic sample of galaxies in the GOODS North field up to $z \sim 3.5$. The sizes of the galaxies are measured from K_s -band images (corresponding to rest-frame optical/NIR) from the Subaru 8 m telescope. We reproduce earlier results based on photometric redshifts that the sizes of galaxies at a given mass evolve with redshift. Specifically, we compare sizes of UV-bright galaxies at a range of redshifts: Lyman-break galaxies (LBGs) selected through the U-drop technique ($z \sim 2.5$ -3.5), BM/BX galaxies at $z \sim 1.5$ -2.5, and *GALEX* LBGs at low redshift ($z \sim 0.6$ -1.5). The median sizes of these UV-bright galaxies evolve as $(1+z)^{-1.11 \pm 0.13}$ between $z \sim 0.5$ and 3.5. The UV-bright galaxies are significantly larger than quiescent galaxies at the same mass and redshift by 0.45 ± 0.09 dex. We also verify the correlation between color and stellar mass density of galaxies to high redshifts. The sizes of submillimeter galaxies in the same field are measured and compared with BM/BX galaxies. We find that the median half-light radius of SMGs is 2.90 ± 0.45 kpc, and there is little difference in their size distribution to the UV-bright star-forming galaxies.

2.1 Introduction

Recent studies provide evidence that sizes of galaxies at high redshifts were smaller in comparison with galaxies of similar mass in the local universe (e.g., Daddi et al. 2005, Trujillo et al. 2006a,b, Zirm et al. 2007, Toft et al. 2007, van Dokkum et al. 2008a, Franx et al. 2008, Williams et al. 2010, Toft et al. 2009, Damjanov et al. 2009, Cimatti et al. 2008, Longhetti et al. 2007). These studies pose several questions about the evolution of properties of galaxies and the build-up of galaxy stellar mass with time. Several physical processes are proposed to explain the growth of galaxies with time, such as galaxy (major or minor) mergers (e.g., Khochfar & Silk 2006, 2009, Bell et al. 2006, Naab et al. 2009), gas accretion in outer regions, and star formation (e.g., Dekel et al. 2009, Elmegreen et al. 2008). However, each of these mechanisms will affect differently the growth of mass and size of galaxies. For example, major dry mergers could produce descendants with larger than observed stellar masses for early-type galaxies. Therefore, some authors (e.g., van Dokkum et al. 2010, Bezanson et al. 2009, Naab et al. 2009, Hopkins et al. 2009) suggest minor mergers and envelope growth by satellite accretion to be a more likely mechanism for building up quiescent galaxies. In general, plausible models have to reproduce galaxy sizes and stellar mass densities seen today and bring the high-redshift galaxies to the local stellar mass-size relation. Therefore, exploring the observed evolution of galaxy sizes is essential to constrain these galaxy formation and evolution models.

However, most of the size studies at high redshift were based on photometric redshifts. Although techniques to construct galaxy spectral energy distributions (SEDs) from multiwavelength observations and photometric redshift measurements are improved over the past few years, photometric redshifts still have worse uncertainties for star-forming galaxies due to the lack of a strong 4000Å break. The large uncertainties and possible systematic biases due to the reliance on photometric redshifts can seriously affect the masses and star formation rate measurements and thus the final results. Spectroscopic observations of high-redshift galaxies and making complete magnitude limited samples require large amounts of observing time. Nevertheless, the advent of 8-10m class telescopes with multi-object spectroscopy has brought about much larger high- z spectroscopic samples than were previously available.

Spectroscopic redshifts are relatively easier to obtain for star-forming galaxies (compare to quiescent galaxies) due to emission lines. Previous results on the size evolution of this population (with photometric redshifts) are interesting since some of the usual mechanisms assumed for size growth, e.g., gas-poor (“dry”) mergers do not apply to gas-rich starburst galaxies since substantial amounts of gas are required for these galaxies to undergo significant star formation. Therefore, studies of the structure of star-forming galaxies with secure redshifts can provide strong constraints on size evolution models.

The actively star-forming galaxies at high redshift consists of two main populations: relatively unobscured UV-bright galaxies and dusty red starbursts, the most extreme of which are detected as submillimetre galaxies (SMGs). The UV-bright galaxies are selected to have strong rest-frame UV. In the past few years, many simple photometric techniques (e.g., “ U -dropout”) were designed to select these galaxies at different redshift ranges (e.g., Steidel et al. 2003, Adelberger et al. 2004).

The SMGs are among the most massive, luminous, and vigorously star-forming galaxies at high redshift that are heavily obscured by dust (e.g., Hughes et al. 1998, Smail et al. 2002, Chapman et al. 2003, 2005). The physical process driving these highly luminous galaxies (star formation, active galactic nucleus (AGN), or combination of these two) is still uncertain. The evolution of SMGs and their relation to the local galaxies are also not yet understood: for instance, whether or not SMGs are the progenitors of local elliptical galaxies (e.g., Blain et al. 2004, Swinbank et al. 2006, Tacconi et al. 2008). Their position on the size-mass plane may therefore provide clues about their relation to other galaxy populations.

To verify previous results based on photometric redshifts, here we study the mass and size evolution of a large sample of UV-bright and SMGs in Great Observatories Origin Deep Survey-North (GOODS-North) with secure spectroscopic redshifts. The structure of this paper is as follows. In Section 2.2, we review the data. In Section 2.3 and 2.4, we describe size and mass determinations of galaxies. Our selected subsamples are described in Section 2.5. Finally, in Section 2.6, we present our results and investigate the size evolution and stellar mass-size relation for our samples. We summarize and discuss our results in Section 2.7. The cosmological parameters adopted throughout this paper are $\Omega_m = 0.3$, $\Omega_\Lambda = 0.7$, and $H_0 = 70 \text{ km s}^{-1} \text{ Mpc}^{-1}$.

2.2 Description of Data

The sample of galaxies used here is based on the most complete spectroscopic catalog of galaxies in the GOODS-North field (Giavalisco et al. 2004) by Barger et al. (2008). This catalog gives a compilation of all spectroscopic observations carried out in this field (e.g., Cowie et al. 2004, Reddy et al. 2006, Wirth et al. 2004, Cohen 2001, Cohen et al. 2000), where each galaxy sample was selected in a different way. In addition, Barger et al. (2008) performed spectroscopic observations for certain subsamples. The catalog includes 2907 sources including stars and is restricted to sources with $K_{s,AB} < 24.5$ or $F850LP_{AB} < 26$. There are 2362 sources with $z < 1.6$ and 327 sources between $z = 1.6$ and 3.5. Most redshifts for galaxies with $z > 1.6$ come from Reddy et al. (2006).

This catalog (Barger et al. 2008) comprises optical photometric data in the F435W, F606W, F775W, and F850LP passbands taken from *Hubble Space Telescope* (HST) Advanced Camera for Surveys (ACS; Giavalisco et al. 2004), and the U -band magnitude is taken from Capak et al. (2004). The near-infrared K_s -band magnitude measured from WIRCam images from the Canada-France-Hawaii Telescope. Details of near-IR observations, data reduction and generating catalog are described more in Barger et al. (2008). X-ray soft (0.5 – 2 KeV) and hard (2 – 8 KeV) luminosities are also provided for many sources in the catalog. In Barger et al. (2008) sources with X-ray luminosities above $10^{42} \text{ ergs s}^{-1}$ in either soft or hard band defined as AGNs. For a fraction of sources ($\sim 36\%$) near-ultraviolet (NUV) and far-ultraviolet (FUV) magnitudes from the UV imaging survey performed by *GALEX* mission were also provided. Note that sources indicated as stars in the catalog are excluded from our analysis.

2.3 Sizes

2.3.1 Size Measurements

Size determination in the observed near-infrared (rest-frame optical at high z) is more robust in tracing the distribution of stellar mass than the observed optical (rest-frame UV at high z) since the sizes at rest-frame UV can be strongly affected by dust and star formation. Therefore, we use K_s -band images from Subaru MOIRCS Deep Survey (MODS) in the GOODS-North field (Kajisawa et al. 2006, Ouchi et al. 2007). The imaging observations are performed for J and K_s bands over ~ 112 arcmin² area of the GOODS-N field with a pixel scale of 0.12 arcsec. We used the images reduced by Bouwens et al. (2008). The resulting FWHM of the K_s images is $\sim 0.5''$. The deepest data cover ~ 28 arcmin² reaching a 5σ of 25.4 AB mag in K_s band while the other regions are ~ 1.3 mag shallower. More details of the images and data reduction can be found in Bouwens et al. (2008).

Sizes of galaxies were estimated by using the GALFIT code (Peng et al. 2002) in a similar procedure used by Trujillo et al. (2007) and Williams et al. (2010). For each galaxy, a square postage stamp of 120 pixels (14.4'') around each galaxy was made, and we use a mask to exclude neighboring galaxies from the fit. A range of Sérsic (1968) profile models convolved with the point-spread function (PSF) of the image are fitted to the K_s images of galaxies. The convolved models for each object were compared with the galaxy surface brightness distribution and the best-fit model determined using minimized χ^2 of the fit. The PSF used by GALFIT was taken from the median of the unsaturated stars over the entire MOIRCS K_s images. We perform a test to check the PSF of the image by measuring sizes of a number of stars in the field listed in the Barger et al. (2008) catalog. The derived sizes of all the stars are found to be $\ll 0.02$ pixel (effectively zero). Therefore, the PSF is a good approximation of a point source. We note that within our K_s -band images, there is a shallower region with seeing of $0.68''$. We followed a similar procedure with an appropriate PSF (which is made from the median of stars in this region) to measure sizes of galaxies in this region separately. We also verified that the derived sizes of the shallower region are reliable by its appropriate PSF.

We determine the circularized effective radius $r_e = a_e \sqrt{(1 - \epsilon)}$, from the half-light radius along the semimajor axis a_e and ellipticity (ϵ) as output by GALFIT. This removes the effects of ellipticity. We allowed the Sérsic index n (which measures the shape of the surface brightness profile of galaxy) to vary between 0.5 and 5 and the effective radius between 0.01 and 60 pixels (0.0012'' and 7.2''). Initial guesses for the effective radius r_e , ellipticity, and position angle were taken from the SExtractor catalog, and magnitude was taken from the original (Barger et al. 2008) catalog, and we set the Sérsic index to 2 initially.

Our results show that the median Sérsic index measured for all galaxies is 2.0 where 50% of measurements lies between 4.0 and 1.0. For galaxies with stellar masses between 10^{10} and $10^{11} M_\odot$, the median Sérsic index is 2.4 where 50% lies between 4.6 and 1.2.

Due to possibility of color gradients, it is best to use the same rest-frame band for measuring sizes of galaxies at all redshifts. However, only deep K imaging is available,

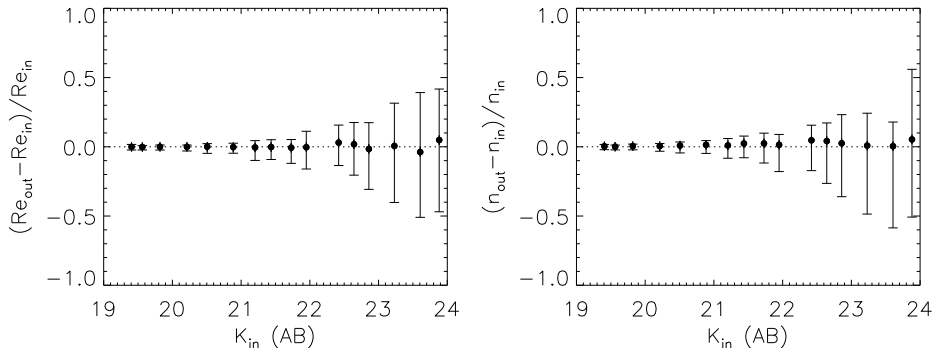


Figure 2.1 – Left panel: the points are the median of the relative difference between the recovered and input sizes vs. magnitude based on our simulations. Right panel: the same comparison, but for the relative difference between output and input Sérsic index. The error bars illustrate the 68% scatter. The random uncertainties of recovered sizes and Sérsic index increase with magnitude.

so there is a possibility of systematic effects with redshift. Franx et al. (2008) show that such systematic effects are small and will not significantly affect the results. As an approximation, we corrected sizes to the rest-frame g band using star-forming galaxies from studies of GOODS-Chandra Deep Field-South (CDF-South; Franx et al. 2008). We derive the best linear fit to the median of the ratio of sizes in K band and rest-frame g band as a function of redshift and apply this fit ($r_{e,k\text{-band}}/r_{e,g\text{-band}} = 0.15z + 0.64$) to galaxies with $z \lesssim 2$ in our sample.

2.3.2 Simulations

To gauge the accuracy of the measured sizes and reliability of our results, we perform a realistic simulation. About 8500 Sérsic profiles were generated with uniformly distributed random parameters in the ranges of $19 < K_{AB} < 25$, $0.1'' < r_e < 2''$, $0.5 < n < 5$ and $0 < \epsilon < 0.8$. The mock galaxies were then convolved with the PSF of the image. Finally, we added these galaxies to 14.4" blank-sky postage stamps randomly taken from our K_s -band image. The structural parameters of the model galaxies were then measured in a manner identical to that used for the actual images.

The results of these simulations are shown in Figures 2.1 and 2.2. The left panel of Figure 2.1 shows that the scatter in the recovered sizes increases with magnitude. The random uncertainties increase significantly after $K_{AB} = 23$. However, the systematic errors are very small ($< 5\%$) even at the faintest magnitudes. Moreover, the simulation shows that the systematic errors on recovery of the Sérsic index are also very small and random uncertainties increase above $K = 23$ (right panel of Figure 2.1). From this result, we limit the sample studied in this paper to galaxies with $K \leq 23$ mag. We note that this

limit is for the deeper region in our K -band images. Running a separate simulation for the shallower region, we find that the derived sizes of galaxies with $K < 22.7$ mag are reliable. Hence, we restricted the sample in this region to this slightly brighter magnitude limit.

We have also explored how the recovery of size depends on the size itself. As shown in Figure 2.2, the uncertainties in retrieving sizes depend on both magnitude and size. Systematic offsets at all magnitudes appear to be negligible except for $r_e > 1.8$ arcsec (which corresponds to 14.4 kpc at $z \sim 1$) at the faintest magnitudes; however, galaxies this large and faint have not been seen at any redshift.

The random uncertainties increase with size in all magnitude bins. For objects with $K_{AB} \leq 20$ mag (top panel), the random uncertainties in size recovery are $< 5\%$. However, for galaxies with $21 < K_{AB} < 22$ the increasing of random uncertainties with sizes is significant. The increase in random uncertainties at larger sizes could be due to decreasing of surface brightness. However, since we are mainly concerned about the overall sample properties, the lack of systematic errors is more important.

2.4 Stellar Mass estimates

The stellar masses of galaxies were measured with the Fitting and Assessment of Synthetic Templates (FAST) code (Kriek et al. 2009). All fluxes from Barger et al. (2008) including four optical bands from ACS, the K_s infrared and U band were used to find the best-fit galaxy template SED to the broadband photometry using a χ^2 minimization procedure. The Bruzual & Charlot (2003) stellar population evolution models with exponentially declining star formation histories (with τ ranging from 10^{7-10} yr) were used to fit the SEDs. We use the Salpeter (1955) initial mass function (IMF) and solar metallicity and the extinction A_V was allowed to vary between 0 and 3. Redshifts of galaxies were fixed to their spectroscopic redshift provided by Barger et al. (2008) catalog. Masses were then shifted by -0.2 dex for consistency with the $z \sim 0$ Sloan Digital Sky Survey (SDSS) masses (which were calculated using a Kroupa 2001 IMF).

2.5 Subsamples

The ability to identify and study distant galaxies has improved dramatically during the last two decades. Various selection criteria have been designed to select high-redshift galaxies through their observed colors. In this paper, we use such criteria to select samples of UV-bright galaxies in redshift ranges of $0.6 \leq z \leq 1.4$, $1.4 \leq z \leq 2.5$ and $2.7 \leq z \leq 3.5$.

Our sample of Lyman-break galaxies (LBGs; $2.7 \leq z \leq 3.5$) is taken from Reddy et al. (2006). Their LBG candidates were originally preselected by the ‘‘C’’, ‘‘D’’, and ‘‘MD’’ criteria which use regions of $(U_n - G)$ versus $(G - R)$ color space (Steidel et al. 2003). Limiting our sample to $K_{AB} \leq 23$, we were only able to include five LBGs in our analysis.

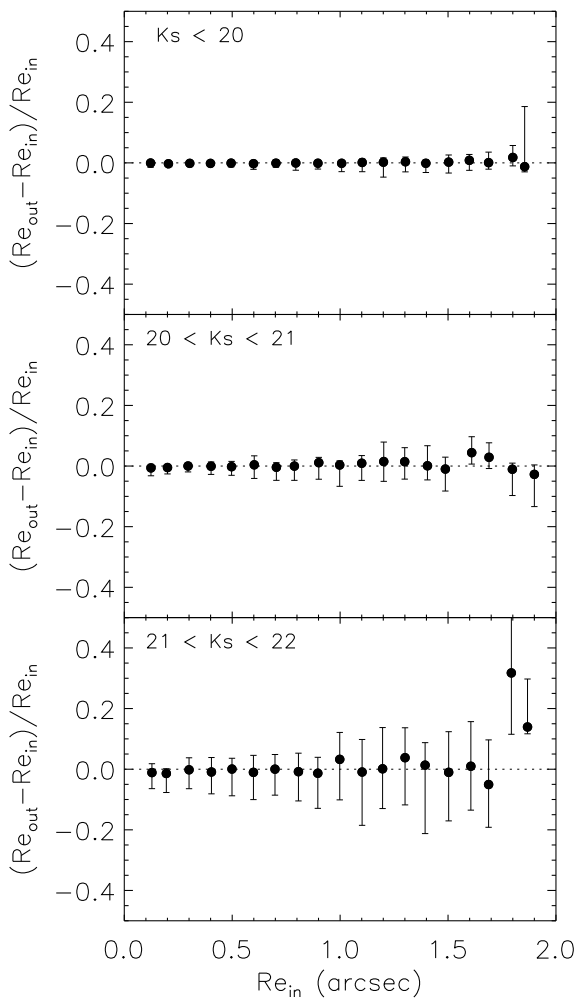


Figure 2.2 – Relative difference between the input and measured sizes of galaxies in our simulations as a function of size for mock galaxies for galaxies with $K_{AB} \leq 20$ mag (top panel), $20 < K_{AB} < 21$ (middle panel), and $21 < K_{AB} < 22$ (lower panel). The relative errors between the input and measured sizes of galaxies as a function of sizes depend on the magnitude.

Table 2.1 – Subsamples

Sample	Redshift	$\log(M_*/M_\odot)$	No. of Sources
BM/BX	$1.4 < z < 2.7$	9.8 - 10.8	41
LBG	$2.7 < z < 3.5$	10.2 - 10.8	5
SMG	$0.5 < z < 3.$	10.0 - 11.7	14
<i>sBzK</i>	$1.4 < z < 3.2$	9.8 - 11.7	70

Notes. Samples of star-forming galaxies studied in this paper.

At $z \sim 2$, BM/BX galaxies also are taken from Reddy et al. (2006). The BM/BX criteria (Adelberger et al. 2004, Steidel et al. 2004) were designed to find actively star-forming galaxies at redshifts $1.4 < z < 2.5$ with similar SEDs to the LBGs. The selection criteria are based on the observed U_nGR colors of galaxies. Reddy et al. (2006) provided spectroscopic observations for candidates brighter than $R_{AB} = 25.5$, photometrically selected from Steidel et al. (2003, 2004). For this paper, 41 BM/BX galaxies to $K_{AB} = 23$ are selected from their sample with spectroscopic redshift $z > 1.4$.

Galaxies analogous to the LBGs at $0.6 \leq z \leq 1.4$ (hereafter *GALEX/LBGs*) are selected with the *GALEX/HST* $(FUV - NUV)_{AB}$ versus $(NUV - F435W)_{AB}$ color-color diagram. Following the selection criteria used in Barger et al. (2008) and requiring $z > 0.6$, we include 105 *GALEX/LBGs* with $K_{AB} \leq 23$.

In addition to the UV-bright galaxies in GOODS-N field, we also study sizes of the SMGs as a population of star-forming galaxies at high redshifts. The subsample of SMGs for our studies is drawn from Chapman et al. (2005) and Pope et al. (2006). The catalog of SMGs provided by Pope et al. (2006) contains 35 candidates from GOODS-N field with 21 secure optical counterparts. Of these, only eight galaxies in our observed images have spectroscopic redshifts. We further include six SMGs from the Chapman et al. (2005) HDF-North study. Therefore, our final SMG sample studied here contains 14 sources spanning $0.5 \leq z \leq 3$.

Besides these two populations, star-forming galaxies at $z > 1.4$ can also be identified using the *BzK* technique (Daddi et al. 2004). This technique is designed to cull galaxies from *K*-selected samples. Star-forming *BzK* galaxies (*sBzK*) tend to be more massive and have higher reddening than UV-selected galaxies. With this method, 70 *sBzK* galaxies at $z > 1.4$ and $K_{AB} \leq 23$ are selected using the criteria $(z - K) - (B - z) > -0.2$. We further use this sample to compare properties of star-forming galaxy populations at high redshifts. The *sBzK* selection criteria can identify $\sim 90\%$ of our BM/BX galaxies. The large overlap is not surprising since both our UV-selected and *sBzK* samples consist of mostly massive galaxies (due to the *K* magnitude limit). Table 2.1 lists samples of star-forming galaxies used in this paper.

2.6 Results

2.6.1 Size Evolution

In Figure 2.3, we show the size distributions for UV-bright galaxies between $10 < \log(M_*/M_\odot) < 11$. The blue histogram shows the measured half-light radii of *GALEX*/LBGs at $z \sim 1$ while the distribution of sizes measured for BM/BX galaxies ($z \sim 2$) is shown as a green histogram. It can be seen from this plot that UV-bright galaxies at $z \sim 2$ are smaller compared to similar galaxies at $z \sim 1$. Specifically, the median half-light radius of BM/BX galaxies in this mass range is 2.68 ± 0.19 kpc significantly smaller than the median effective radii of *GALEX*/LBGs (4.42 ± 0.52 kpc). This means that sizes of UV-bright galaxies evolve by a median factor of 0.60 ± 0.08 between $z \sim 2$ and $z \sim 1$. It is harder to measure the evolution for $z \sim 3$ to $z \sim 2$, as we have four LBGs within mass range of $10 < \log(M_*/M_\odot) < 11$ at $z \sim 3$ in our sample. The median half-light radius of these four massive galaxies is 2.22 ± 0.61 kpc, 0.82 ± 0.23 smaller than $z \sim 2$ BM/BX galaxies. We perform a power-law fit on the size evolution and find $r_e \propto (1+z)^{-1.11 \pm 0.13}$ over the range $0.6 \lesssim z \lesssim 3.5$.

The size-redshift relation for star-forming galaxies with spectroscopic redshifts in the GOODS-North field is shown in Figure 2.4. Galaxies are split into the four different stellar mass bins shown in the figure. In each panel, the gray small symbols are normal star-forming galaxies with spectroscopic redshifts selected to have specific star formation rates $\log \text{sSFR} > -10$. Color symbols represent our samples of UV-bright galaxies and SMGs. LBGs ($2.7 < z < 3.5$) are shown as dark-green triangles, and BM/BX galaxies ($1.4 < z < 2.7$) are plotted as green squares. *GALEX*/LBGs at relatively lower redshifts ($0.6 < z < 1.4$) are plotted in different panels as blue stars. The black symbols at $z \sim 0$ are star-forming galaxies from Guo et al. (2009) from SDSS.

As Figure 2.4 shows, sizes of UV-bright galaxies at a fixed stellar mass increase toward lower redshifts. There is also a trend that the size evolution maybe stronger for the most massive galaxies. For example, UV-bright galaxies with stellar masses $9 < \log(M_*/M_\odot) < 10$ evolve by a median factor of approximately 1.15 ± 0.25 from $z \sim 2$ to $z \sim 0.8$. However, galaxies with masses $10 < \log(M_*/M_\odot) < 10.5$ grow by a median factor of approximately 1.82 ± 0.25 . At higher stellar mass bin ($10.5 < \log(M_*/M_\odot) < 11$), this evolution is even stronger: a factor of 2.05 ± 1.26 over the same redshift range. However, selection effects may influence this trend (especially in the low-mass bin) and more complete samples are needed.

SMGs are also shown as pink diamonds in Figure 2.4; they are discussed further in Section 2.6.4. Galaxies which have X-ray luminosities $> 10^{42}$ ergs s^{-1} (i.e., potential AGN hosts) are marked with open circles. These galaxies have sizes similar to the others. Since AGN is point-like, one would expect galaxies with AGN emission to have smaller half-light radii. Their “normal” rest-frame optical sizes are thus perhaps not strongly influenced. Nonetheless, due to possible effects on the size and mass estimates, X-ray-detected galaxies should be considered low-confidence points.

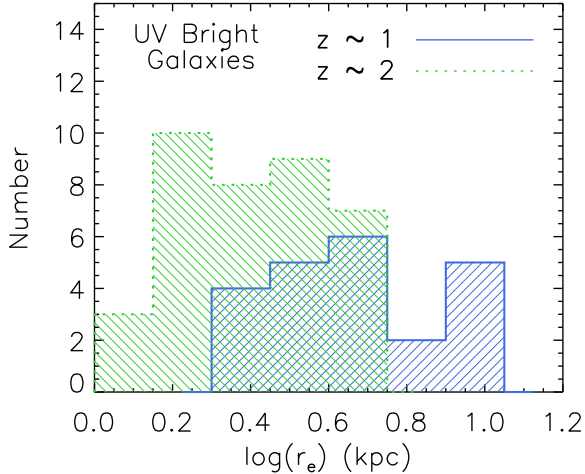


Figure 2.3 – Size distribution of UV-bright galaxies with stellar mass $10 < \log(M_*/M_\odot) < 11$ at $z \sim 1$ (blue histogram) and $z \sim 2$ (green histogram). The half-light radii of UV-bright galaxies (*GALEX*(LBGs)) at $z \sim 1$ are larger than BM/BX galaxies at $z \sim 2$.

2.6.2 Stellar Mass-Size Relation

We now investigate how mass-size distribution of the UV-bright galaxies compares to other galaxy populations. We further check if the relation between stellar mass and size of these galaxies exists to high redshift.

The stellar mass-size distributions of our samples are shown in Figure 2.5. We have divided our sample into three redshift bins: $0.5 < z < 1.5$, $1.5 < z < 2.5$, and $2.5 < z < 3.5$. UV-bright galaxies are color coded in the same way as in Figure 2.4. Solid and dotted lines in each panel show the mass-size relation from Shen et al. (2003) for star-forming galaxies and early-type galaxies at $z \sim 0$, respectively. The gray symbols are the *K*-selected sample of galaxies in CDF-South with stellar masses $> 10^{9.8} M_\odot$ (Franx et al. 2008). Comparing our results with the galaxies from CDF-S allows us to see where our galaxies lie relative to a purely mass-selected sample. Brown solid lines in the middle of each panel show the median effective radii in narrow mass bins for all galaxies in CDF-S. As can be seen, at $z \sim 1$ and $z \sim 2$, UV-bright galaxies have larger effective radii compared to all galaxies at a given stellar mass. For galaxies between 10^{10} and $10^{11} M_\odot$, the median sizes differ by a factor of 1.89 ± 0.23 and 1.12 ± 0.09 at $z \sim 1$ and 2, respectively. As the spectroscopic sample contains only four UV-bright galaxies in this mass range at $z \sim 3$, the difference with CDF-S is not well constrained at this redshift (1.27 ± 0.36).

We further investigate how the size-mass distribution of GOODS-N UV-bright galaxies compares to that of UV-bright galaxies in CDF-S. This would help to verify if the

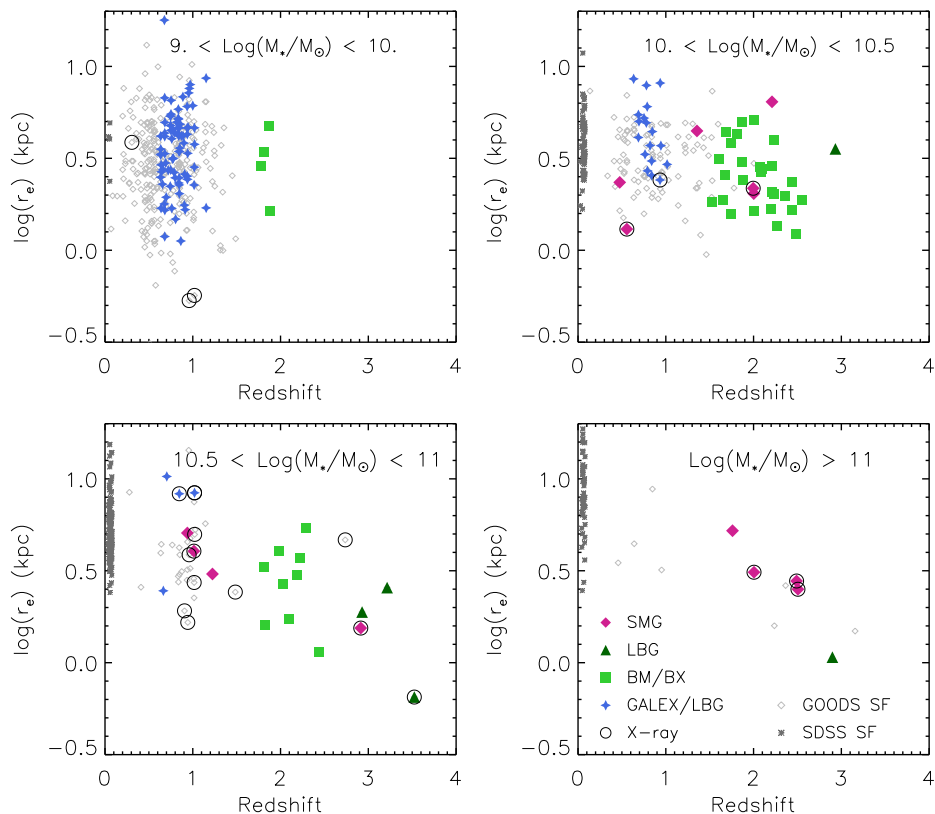


Figure 2.4 – Evolution of sizes of galaxies as a function of redshift. Each panel shows the size evolution for a narrow stellar mass bin. The gray symbols are star-forming galaxies with spectroscopic redshifts in GOODS-N field. Blue stars are GALEX/LBGs ($z \sim 1$) while the green squares and green triangles represent BM/BX galaxies ($z \sim 2$) and LBGs ($z \sim 3$), respectively. SMGs are also shown as pink diamonds. Galaxies with X-ray luminosities more than 10^{42} ergs s^{-1} are marked by open circles. Black symbols at $z \sim 0$ are SDSS star-forming galaxies from Guo et al. (2009). As this plot illustrates, the half light radii of UV-bright galaxies evolve with redshift and this evolution is faster for high-mass galaxies.

previously reported size-mass relation for a large photometric sample (Franx et al. 2008) is consistent with our spectroscopic sample. We define analogs of the $z \sim 1, 2,$ and 3 LBGs in CDF-S by their optical colors and magnitudes. Specifically, we selected the analogs of the $z \sim 1$ *GALEX*/LBGs by requiring $(B - V) < 0.6$ and $R \leq 23.8$. This selection is based on the locus of the GOODS-N *GALEX*/LBGs in this color-magnitude plane. The analogs of BM/BX galaxies in CDF-S are similarly selected with $R < 25.1$ and $(B - V) < 0.8$ and $z_{phot} = 1.5 - 2.5$. We note that the R -band magnitude in both surveys is estimated by the average values of V - and I -band magnitudes. We verified that the spectroscopic samples are effectively selected by these criteria. In order to identify analogs of UV-bright objects in CDF-S at $z \sim 2.5 - 3.5$, we find the location of LBGs in GOODS-N on the color-color $(B - V)$ versus $(V - I)$ diagram and apply the following criteria to the CDF-S galaxies: (1) $0.5 < (B - V) < 1.2$ for $(V - I) < 0.35$; (2) $(B - V) > 3 \times (V - I) + 0.5$ and $(B - V) < 1.2$ for $0.35 < (V - I) < 0.5$. We note that these selection criteria do not impose a ‘‘U-drop out’’ criteria, but do select galaxies with similar brightness and UV slope as the usual LBG methods.

The comparison of size-mass distributions for UV-bright galaxies from both fields is shown in Figure 2.6. In each panel, the color symbols are the median log effective radii of UV-bright galaxies in narrow mass bins, with the blue and green symbols representing UV-bright galaxies in GOODS-N and the brown symbols are the ones in CDF-S. The error bars show the 1σ dispersion. UV-bright samples from both fields follow consistent size-mass relation, further confirming that UV-bright galaxies are on average larger than overall galaxies at a fixed stellar mass. We note that at high redshift ($z \sim 2.5 - 3.5$) the comparison is weak because of the limited number LBGs in GOODS-N.

The UV-bright galaxies show a weak stellar mass-size relation at $z = 1$ and $z = 2$ in Figure 2.5. To quantify this relation, we fitted a power-law function of the form $r_e \propto M^\alpha$ to the individual UV-bright galaxies in each redshift bin. The fitting results are plotted as color dashed-dotted lines in Figure 2.6. At $z \sim 1$, the size of *GALEX*/LBGs in GOODS-N scales with stellar mass as $r_e \propto M^{0.19 \pm 0.05}$ and the BM/BX galaxies at $z \sim 2$ have $r_e \propto M^{0.30 \pm 0.06}$. The uncertainties were estimated using bootstrap resampling. The results are comparable to the relation for late-type galaxies at $z \sim 0$ from Shen et al. (2003). They found $r_e \propto M^{0.15}$ for low-mass ($\log(M) < 10.6$) late-type galaxies and steeper relation for high-mass late-type galaxies ($r_e \propto M^{0.4}$). In the highest redshift bin ($z \sim 3$), we use UV-bright galaxies from CDF-S to find the best fit ($\alpha = 0.32 \pm 0.06$). Table 2.2 lists the best-fit power-law parameter to the mass-size relation of UV-bright galaxies. The slopes of the mass-size relation at different redshift bins are consistent and there is no significant evolution. Our results confirm the persistence of the size-mass relation for star-forming galaxies up to high redshift.

It is worth checking whether or not other star-forming populations at high redshift have the same size-mass relation. Therefore, we compare star-forming *BzK* galaxies (*sBzK*) with BM/BX galaxies. The size distribution as a function of stellar mass is shown in Figure 2.7 with the *sBzK* galaxies plotted as gray filled circles. The medians of log effective radii of *sBzK* galaxies are overplotted as red squares. BM/BX galaxies and SMGs are marked with the green and pink circles, respectively, and the green dashed-dotted line shows the mass-size relation for BM/BX galaxies. As one can see, the mass-size relation

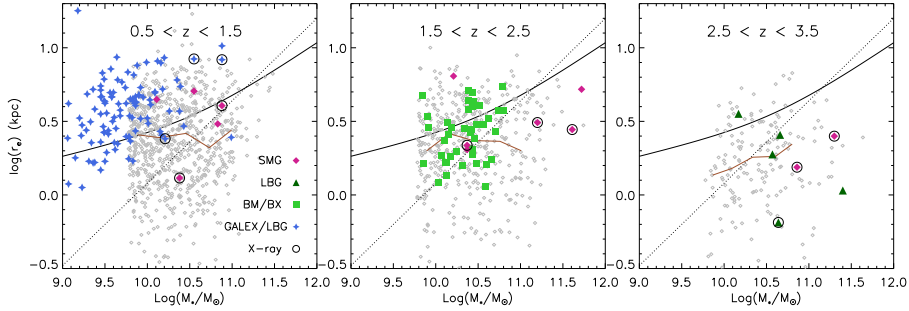


Figure 2.5 – Stellar mass-size distribution for UV-bright galaxies in different redshift bins compared to the galaxies from CDF-South (Franx et al. 2008) (gray dots). The color symbols represented here are the same as Figure 2.4. The solid and dotted black lines are the size-mass relations for star-forming and quiescent galaxies, respectively, at $z \sim 0$ from Shen et al. (2003). The solid brown lines show the median sizes in narrow mass bins for all galaxies from CDF-S. The UV bright galaxies are in general larger than normal field galaxies at the same mass.

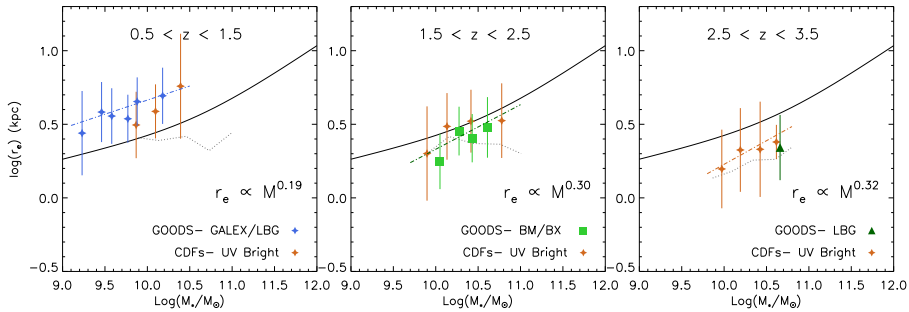


Figure 2.6 – Comparison of the stellar mass-size relation for the UV-bright galaxies from GOODS-N field and CDF-South in three redshift bins. The black solid lines are the size-mass relation for star-forming galaxies at $z \sim 0$ from Shen et al. (2003). The color symbols are median of UV-bright galaxies in narrow mass bins and the error bars show 1σ (68%) dispersion. The dashed-dotted lines are the best power-law fits using $r_e \propto M^\alpha$ to the individual UV-bright galaxies. The dotted lines are the median sizes in narrow mass bins for all galaxies from CDF-S (Same as Figure 2.5). This plot shows that the derived half-light radii of UV-bright galaxies from both fields are in place and agreement with each other up to $z \sim 3$.

Table 2.2 – Best Fits Power-law Parameter for the Stellar Mass-Size Relation

Sample	Redshift	α
<i>GALEX</i> /LBG	$0.6 < z < 1.4$	0.19 ± 0.05
BM/BX	$1.4 < z < 2.7$	0.30 ± 0.06
CDFs-UV Bright	$2.5 < z < 3.5$	0.32 ± 0.06
<i>sBzK</i>	$1.4 < z < 3.2$	0.31 ± 0.09

Notes. Power-law parameter α is defined as $r_e \propto M_*^\alpha$.

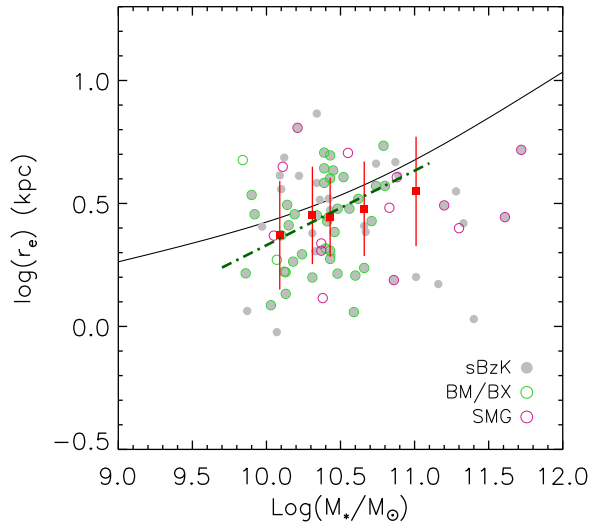


Figure 2.7 – Stellar mass-size relation for star-forming *sBzK* galaxies (gray circles). The BM/BX galaxies and SMGs are marked with green and pink circles, respectively. The red squares are the median for the mass-size relation of *sBzK* sample with 1σ dispersion. The green dashed-dotted line is the best fit to the BM/BX galaxies. The *sBzK* galaxies have a similar size-mass relation to the BM/BX galaxies. The solid line shows the mass-size relation for star-forming galaxies at $z \sim 0$ from Shen et al. (2003).

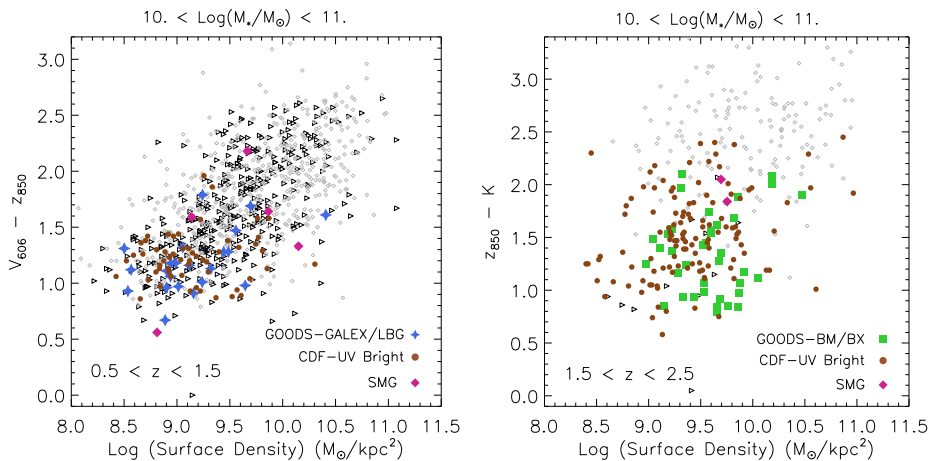


Figure 2.8 – Left panel: the correlation between color ($V_{606} - z_{850}$) and surface density for galaxies in the redshift range of $0.5 < z < 1.5$ and stellar masses $10^{10} < M/M_{\odot} < 10^{11}$ in GOODS-N field. The blue stars are *GALEX*(LBGs) from GOODS-N and the brown circles are from CDF-S. The gray symbols are all galaxies from CDFS and the black triangles are galaxies from GOODS-N. Right panel: the color ($z_{850} - K$) vs. surface density for galaxies at $1.5 < z < 2.5$, as the green squares are the BM/BX galaxies from GOODS-N and the brown circles are pseudo-BM/BX from CDF-S. The plots indicate that blue galaxies having lower surface density.

for $sBzK$ galaxies is comparable to the one for BM/BX galaxies. The average offset of median half-light radii of $sBzK$ galaxies to the BM/BX mass-size relation is 0.037 dex. The effective radii of $sBzK$ galaxies scale with stellar mass as $r_e \propto M^{0.31 \pm 0.09}$ close to the size-mass relation for UV-bright galaxies. This similarity could be due to the significant overlap between the UV-selected galaxies and $sBzK$ galaxies (e.g., Reddy et al. 2005). We note that stellar masses can have significant uncertainties depending on the methods used to calculate them. We verify that by using the stellar mass estimates from Reddy et al. (2006) for UV-bright galaxies, the size-mass distribution of these galaxies covers the same region in the size-mass plane (see, e.g., the middle panel of Figure 2.5). Hence, this shows that our results are robust against using different estimates of stellar masses.

2.6.3 Color-Surface Density

One of the surprising results of Franx et al. (2008) was the tight correlation between stellar mass surface density (M_*/r_e^2) and color of galaxies to $z \sim 3$. They showed that bluer galaxies have lower surface densities than red quiescent ones. They indicated that the color of galaxies correlates more fundamentally with the stellar mass surface density than the mass.

We show the tight relation between color and stellar mass surface density for both star-forming and quiescent galaxies with $M_{\odot} \sim 10^{10} - 10^{11}$ in Figure 2.8. In the left panel, the

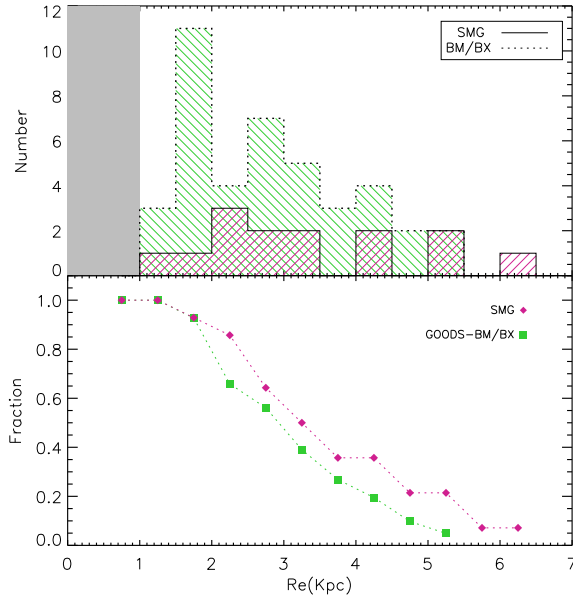


Figure 2.9 – Top panel: histograms show the distribution of sizes of SMGs (solid line) and BM/BX galaxies (dotted lines). The gray region indicates apparent effective radii below $0.1''$ (~ 1 kpc at $z \sim 2$) which size measurements have large uncertainties. Lower panel: cumulative distribution function for SMGs (pink diamonds) and BM/BX galaxies (green squares). As the plot shows, the distributions of half-light radii of these two populations are comparable with SMGs being slightly larger.

observed color ($V_{606} - z_{850}$) is plotted versus the stellar mass surface density for galaxies at redshift ~ 1 . The black and gray symbols are galaxies from GOODS-N and CDF-S fields, respectively. The blue stars and brown circles indicate the *GALEX* (LBGs) and their analogs from CDF-S, respectively. In the right panel, the relation between observed ($z_{850}-K$) and surface density for galaxies at higher redshift ~ 2 is illustrated, with BM/BX galaxies in GOODS-N shown by green squares and their analogs in CDF-S as brown circles. As can be seen in this figure, the blue star-forming galaxies have lower surface density than red galaxies at both $z \sim 1$ and $z \sim 2$, though the correlation between color and surface density is more tight at $z \sim 1$ than $z \sim 2$. In general, using sample of galaxies with spectroscopic redshifts confirms that the color of galaxies tightly correlates with surface density and this relation holds out to high redshifts.

2.6.4 Sizes of Submillimeter Galaxies

Since GOODS-N includes 14 SMGs with redshifts, we compare their masses and sizes to the UV-selected galaxies at $z \sim 2$. As Figure 2.4 illustrates, the optical rest-frame sizes of the SMGs (pink diamonds) and UV-selected galaxies of similar mass are comparable. The median half-light radius of all SMGs is 2.90 ± 0.45 kpc which is in good agreement with the median optical rest-frame sizes of the BM/BX galaxies over the whole mass range (2.68 ± 0.25 kpc). The median effective radius of SMGs with stellar masses of 10^{10} - 10^{11} is 2.65 ± 0.56 which is similar to the BM/BX of at the same mass range (2.68 ± 0.19). The errors are computed using bootstrap resampling.

We further compare the size distributions of SMGs and BM/BX galaxies in Figure 2.9. In the top panel, the histograms show the size distribution of BM/BX galaxies and SMGs. In the bottom panel, the normalized cumulative distribution functions are shown for both samples. As this plot shows, the size distributions of SMGs are comparable with $z \sim 2$ UV-bright galaxies and the SMGs follow the same size distribution as BM/BX galaxies in the optical rest-frame with SMGs being slightly larger. According to a K-S test, the probability that two distributions being the same is 72%, suggesting no significant difference between the rest-frame optical sizes of the SMGs and UV-bright galaxies.

2.7 Discussion

2.7.1 The growth of star-forming galaxies

We study the size evolution of galaxies with spectroscopic redshifts between $z \sim 0.5$ and 3.5. Our results are summarized in Figure 2.10. As this plot illustrates, at each epoch, the median sizes of UV-bright galaxies (color squares) with stellar masses $10 < \log(M_*/M_\odot) < 11$ are larger (by a median factor of 0.45 ± 0.09) than quiescent galaxies in a similar mass range selected from CDF-S (red circles). The red triangle is the median sizes of quiescent galaxies studied in (van Dokkum et al. 2008, VD08 hereafter) with a median stellar mass of $1.7 \times 10^{11} M_\odot$ and median redshift of 2.3. Table 2.3 lists the median half-light radii for UV-bright and quiescent galaxies seen in Figure 2.10. The growth of UV-bright galaxies with time is also illustrated in this figure. The dashed line shows that UV-bright galaxies scaled up their sizes toward lower redshifts as $(1+z)^{-1.11 \pm 0.13}$.

Previous studies (Franx et al. 2008, Kauffmann et al. 2003) have reported that there is a correlation between color and stellar mass surface density of galaxies at both low and high redshifts. However, the results based on photometric redshifts can be uncertain especially for star-forming galaxies. By means of our large sample of galaxies with secure redshifts, we have confirmed that the tight correlation between color and stellar mass surface density of galaxies that holds out to high redshifts; as the stellar mass densities of blue star-forming galaxies are smaller than those of red quiescent ones. This verifies that the galaxies with higher specific star formation rate are larger than the ones with lower specific star formation rates.

We have also explored the stellar mass-size distribution for galaxies in our sample. We have confirmed that there is a relation between stellar mass and size for UV-bright galaxies

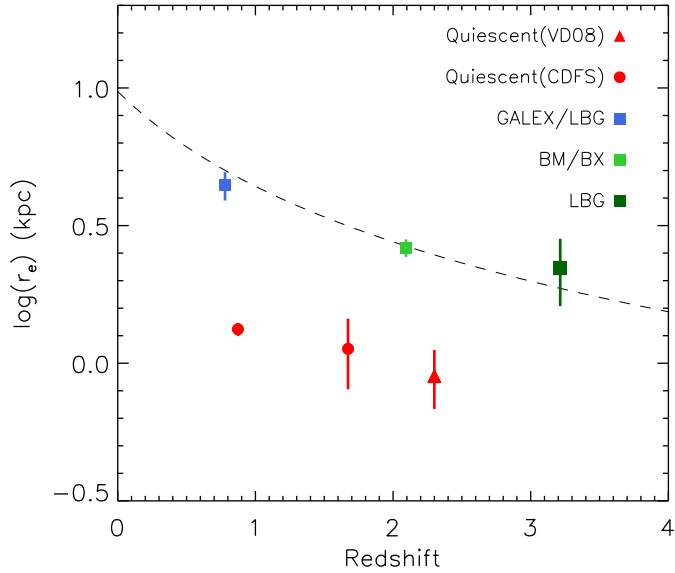


Figure 2.10 – Median sizes of UV-bright galaxies (squares) as a function of redshifts for galaxies with stellar masses $10^{10} < M/M_{\odot} < 10^{11}$ in GOODS-N field. The red filled circles are quiescent galaxies from CDF-S study with similar mass range and the red triangle is the quiescent sample from van Dokkum et al. (2008) with median stellar masses of $1.7 \times 10^{11} M_{\odot}$. The dashed line shows the best-fitting size evolution to the UV-bright galaxies ($r_e \propto (1+z)^{-1.11 \pm 0.13}$). The plot indicates that the UV-selected galaxies are larger than quiescent galaxies and their sizes evolve with redshift.

at $0.5 < z < 3.5$. The relations are consistent for both spectroscopic and photometric redshift samples. Our results verify that there is no significant evolution of the slope of the size-mass relation to redshift ~ 3.5 . The evolution of the relation from $z = 1$ to $z = 0$ is not well established, as it is not straight forward to select LBGs at $z \sim 0$. Some authors find evolution (e.g., Franx et al. 2008, Williams et al. 2010) in the stellar mass-size relation; however, Barden et al. (2005) have reported that the stellar mass-size relation for disk galaxies remains constant from $z \sim 1$ to the present. Selection effects likely play a role. Comparing to the theoretical work, the size evolution predicted by Somerville et al. (2008) is somewhat stronger than the evolution we measured here.

Star-forming galaxies at high redshifts can be identified by means of different methods of sample selection and can be assigned as different populations of galaxies (e.g., submillimeter or *sBzK*) and therefore studied separately. However, many of these galaxy populations may overlap, hence it is worth checking out if they have comparable properties. We, therefore, compare sizes of UV-bright galaxies to other types of star-forming galaxy populations at high redshift, i.e., *sBzK* galaxies and SMGs. We show that these two populations have comparable sizes to the UV-bright galaxies. This suggests that, in general, star-forming galaxies have larger sizes than quiescent ones without regard to their type. However, sample selection might alter the results. We return to this possibility later, in Section 2.7.3.

2.7.2 Comparison to previous work

The strong growth of both star-forming and quiescent galaxies has been shown by several authors (Trujillo et al. 2006b, Franx et al. 2008, Williams et al. 2010, Toft et al. 2007). The size growth of star-forming galaxies studied here going as $(1+z)^\alpha$, where $\alpha = -1.11 \pm 0.13$, agrees well compared to previous studies where the size evolves with $\alpha \sim -1$. For example, Bouwens et al. (2006) found $\alpha = -1.1 \pm 0.3$ for a sample of luminosity-selected dropout galaxies between $z \sim 6$ and $z \sim 2.5$, while Dahlen et al. (2007) found $\alpha = -1.10 \pm 0.07$ for luminosity-selected disk galaxies over the range $z \sim 1.1$ -2.2. Williams et al. (2010) also found a similar slope for star-forming galaxies in UDS at $z \sim 0.5$ -2.

The similarity between sizes of UV-bright galaxies and star-forming *BzK* galaxies is also shown in our study. The two populations are also compared by Overzier et al. (2010). They showed that rest-frame optical sizes of *sBzK* galaxies are somewhat larger than UV-selected galaxies. Since *BzK* galaxies are K-selected and thus tend to represent massive galaxies, it is not surprising that they appear larger. Hence, the sizes must be corrected for differing stellar masses for an accurate comparison to be made.

Our results also show that the SMGs have a median half-light radius of 2.90 ± 0.45 kpc comparable to the rest-frame optical sizes of the BM/BX galaxies. The result is in agreement with a recent study by Swinbank et al. (2010) where they use deep *HST I* and *H*-band imaging and show that the rest-frame optical sizes of the SMGs and UV-bright galaxies in GOODS-N are comparable. The typical half-light radius of the SMGs in the *H*-band (rest-frame optical) measured by Swinbank et al. (2010) is 2.8 ± 0.4 which is consistent with our measurements (see also Targett et al. 2010 for more comparison.). Almaini et al. (2005) also compared sizes of SMGs with LBGs at rest-frame optical and

Table 2.3 – Median Sizes of Different Samples

Sample	Redshift	Median Size (kpc)	Median($\log(M_*/M_\odot)$)
<i>GALEX</i> /LBG	$0.6 < z < 1.4$	4.42 ± 0.52	10.2 ± 0.3
BM/BX	$1.4 < z < 2.7$	2.68 ± 0.19	10.4 ± 0.2
LBG	$2.7 < z < 3.5$	2.22 ± 0.61	10.6 ± 0.2
CDFS	$0.5 < z < 1.5$	2.33 ± 0.1	10.4 ± 0.3
CDFS	$1.5 < z < 2.5$	2.40 ± 0.13	10.4 ± 0.3
CDFS	$2.5 < z < 3.5$	1.73 ± 0.18	10.4 ± 0.3
Quiescent(CDFS)	$0.5 < z < 1.5$	1.32 ± 0.07	10.5 ± 0.3
Quiescent(CDFS)	$1.5 < z < 2$	1.12 ± 0.32	10.7 ± 0.2
Quiescent(VD08)	$2 < z < 2.5$	0.9 ± 0.21	11.23
SMG	$0.5 < z < 3.$	2.90 ± 0.45	10.8 ± 0.5

Notes. The median sizes are for galaxies with stellar masses between 10^{10} and $10^{11} M_\odot$. This mass limit is not applied to the quiescent (van Dokkum et al. 2008, , VD08) and SMG galaxies. The CDFS samples contain both star-forming and quiescent galaxies at the same mass range in CDF-S.

found no clear difference between sizes of the SMGs and LBGs. It is worth noting that SMGs have larger median stellar masses compared to BM/BX galaxies (also mentioned in Swinbank et al. 2010). This suggests higher stellar mass densities for SMGs compared to UV bright galaxies. However, the similarity in sizes between these two galaxy populations at high z does not by itself allow conclusive connections to be drawn between the two populations. The SMGs that are faint or lacking emission lines could be missing from our spectroscopic sample and they may have dramatically different mass or size properties. Therefore, selection effect could bias these results. Spectroscopic observation in near-IR might help to solve this problem; e.g., Kriek et al. (2009a) find a median size of 2.8 kpc for a small sample of near-IR spectroscopically confirmed star-forming galaxies at $z \sim 2.3$. Indeed, our measured size evolution is consistent with their spectroscopic sample; however, near-IR spectroscopy over a large redshift range is needed to definitively quantify the size evolution.

2.7.3 Caveats

With this large spectroscopic sample of high-redshift galaxies, we have removed an important source of uncertainty in the stellar mass-size relation and verified the results from larger samples based on photometric redshifts. However, the spectroscopic catalog we used in this study consists of many different spectroscopic surveys which made it inhomogeneous. Galaxies in this catalog are mostly relatively unobscured star-forming galaxies with emission lines, comparing these to quiescent galaxies can still be a problem because spectroscopy of high-redshift red galaxies is difficult. Therefore, using a larger and homogeneous sample of high-redshift galaxies with secure redshift will allow greatly

improved constraints on their evolution. New ground and space-based IR multi-object spectrographs (WFC3 grism, MMIRS, MOSFIRE) will allow investigations of more complete samples of galaxies and study the correlation between galaxy properties at higher redshifts. Dust-obscured starbursts are also likely to be missed in our UV-bright sample, hence NIR spectroscopy will also permit studies of this important population.

2.8 Summary

We have performed the first size evolution study of UV-bright galaxies with secure redshifts in the GOODS-North field. We derive half-light radii of galaxies at a wide range of redshifts (up to $z \sim 3.5$). Using sample of galaxies with secure redshifts, we have quantified the size evolution of galaxies without the potential uncertainty of photometric redshifts and confirm the previous studies that galaxies of similar mass were generally smaller at past and their sizes evolve with redshift. Specifically, we find that:

- UV-bright galaxies evolve strongly as $(1 + z)^{-1.11 \pm 0.13}$ confirming previous studies based on photometric redshifts (e.g., Trujillo et al. 2006b, 2007, Franx et al. 2008, Williams et al. 2010).
- UV-bright galaxies are significantly larger than quiescent galaxies. At the same mass, the median difference is 0.45 ± 0.09 dex.
- The LBG, BM/BX, and *GALEX*/LBG samples show smooth evolution with redshift, indicating that these techniques indeed select similar UV-bright galaxies at different redshifts.
- The SMGs have half-light radii similar to UV-bright galaxies of the same mass.

2.9 Acknowledgments

We thank anonymous referee for helpful comments and suggestions. We thank Rychard Bouwens for providing us *K*-band images. M.M. is supported by the Marie Curie Initial Training Network ELIXIR (Early unIverse eXploration with nIRspec), grant agreement PITN-GA-2008-214227 (from the European Commission). R.J.W. acknowledges support from the Nederlandse Onderzoekschool voor Astronomie (NOVA) and NSF grant AST-0707417.

Bibliography

- Adelberger, K. L., Steidel, C. C., Shapley, A. E., Hunt, M. P., Erb, D. K., Reddy, N. A., & Pettini, M. 2004, *ApJ*, 607, 226
- Almaini, O., Dunlop, J. S., Conselice, C. J., Targett, T. A., & Mclure, R. J. 2005, arXiv:astro-ph/0511009v1
- Barden, M., et al. 2005, *ApJ*, 635, 959
- Barger, A. J., Cowie, L. L., & Wang, W. 2008, *ApJ*, 689, 687
- Bell, E. F., et al. 2006, *ApJ*, 640, 241
- Bezanson, R., van Dokkum, P. G., Tal, T., Marchesini, D., Kriek, M., Franx, M., & Coppi, P. 2009, *ApJ*, 697, 1290
- Blain, A. W., Chapman, S. C., Smail, I., & Ivison, R. 2004, *ApJ*, 611, 725
- Bouwens, R. J., Illingworth, G. D., Blakeslee, J. P., & Franx, M. 2006, *ApJ*, 653, 53
- Bouwens, R. J., Illingworth, G. D., Franx, M., & Ford, H. 2008, *ApJ*, 686, 230
- Bruzual, G., & Charlot, S. 2003, *MNRAS*, 344, 1000
- Capak, P., et al. 2004, *AJ*, 127, 180
- Chapman, S. C., Blain, A. W., Ivison, R. J., & Smail, I. R. 2003, *Nature*, 422, 695
- Chapman, S. C., Blain, A. W., Smail, I., & Ivison, R. J. 2005, *ApJ*, 622, 772
- Cimatti, A., et al. 2008, *A&A*, 482, 21
- Cohen, J. G. 2001, *AJ*, 121, 2895
- Cohen, J. G., Hogg, D. W., Blandford, R., Cowie, L. L., Hu, E., Songaila, A., Shopbell, P., & Richberg, K. 2000, *ApJ*, 538, 29
- Cowie, L. L., Barger, A. J., Hu, E. M., Capak, P., & Songaila, A. 2004, *AJ*, 127, 3137
- Daddi, E., Cimatti, A., Renzini, A., Fontana, A., Mignoli, M., Pozzetti, L., Tozzi, P., & Zamorani, G. 2004, *ApJ*, 617, 746
- Daddi, E., et al. 2005, *ApJ*, 626, 680
- Dahlen, T., Mobasher, B., Dickinson, M., Ferguson, H. C., Giavalisco, M., Kretchmer, C., & Ravindranath, S. 2007, *ApJ*, 654, 172
- Damjanov, I., et al. 2009, *ApJ*, 695, 101
- Dekel, A., Sari, R., & Ceverino, D. 2009, *ApJ*, 703, 785
- Elmegreen, B. G., Bournaud, F., & Elmegreen, D. M. 2008, *ApJ*, 688, 67
- Franx, M., van Dokkum, P. G., Schreiber, N. M. F., Wuyts, S., Labbé, I., & Toft, S. 2008, *ApJ*, 688, 770
- Giavalisco, M., et al. 2004, *ApJ*, 600, L93
- Guo, Y., et al. 2009, *MNRAS*, 398, 1129
- Hopkins, P. F., Bundy, K., Murray, N., Quataert, E., Lauer, T. R., & Ma, C. 2009, *MNRAS*, 398, 898
- Hughes, D. H., et al. 1998, *Nature*, 394, 241
- Kajisawa, M., et al. 2006, *PASJ*, 58, 951
- Kauffmann, G., et al. 2003, *MNRAS*, 341, 54

- Khochfar, S., & Silk, J. 2006, *ApJ*, 648, L21
—, 2009, *MNRAS*, 397, 506
- Kriek, M., van Dokkum, P. G., Franx, M., Illingworth, G. D., & Magee, D. K. 2009a, *ApJ*, 705, L71
- Kriek, M., van Dokkum, P. G., Labbé, I., Franx, M., Illingworth, G. D., Marchesini, D., & Quadri, R. F. 2009b, *ApJ*, 700, 221
- Kroupa, P. 2001, *MNRAS*, 322, 231
- Longhetti, M., et al. 2007, *MNRAS*, 374, 614
- Naab, T., Johansson, P. H., & Ostriker, J. P. 2009, *ApJ*, 699, L178
- Ouchi, M., Tokoku, C., Shimasaku, K., & Ichikawa, T. 2007, in *Astronomical Society of the Pacific Conference Series*, Vol. 379, *Cosmic Frontiers*, ed. N. Metcalfe & T. Shanks, 47–+
- Overzier, R. A., Heckman, T. M., Schiminovich, D., Basu-Zych, A., Gonçalves, T., Martin, D. C., & Rich, R. M. 2010, *ApJ*, 710, 979
- Peng, C. Y., Ho, L. C., Impey, C. D., & Rix, H. 2002, *AJ*, 124, 266
- Pope, A., et al. 2006, *MNRAS*, 370, 1185
- Reddy, N. A., Erb, D. K., Steidel, C. C., Shapley, A. E., Adelberger, K. L., & Pettini, M. 2005, *ApJ*, 633, 748
- Reddy, N. A., Steidel, C. C., Erb, D. K., Shapley, A. E., & Pettini, M. 2006, *ApJ*, 653, 1004
- Salpeter, E. E. 1955, *ApJ*, 121, 161
- Shen, S., Mo, H. J., White, S. D. M., Blanton, M. R., Kauffmann, G., Voges, W., Brinkmann, J., & Csabai, I. 2003, *MNRAS*, 343, 978
- Smail, I., Ivison, R. J., Blain, A. W., & Kneib, J. 2002, *MNRAS*, 331, 495
- Somerville, R. S., et al. 2008, *ApJ*, 672, 776
- Steidel, C. C., Adelberger, K. L., Shapley, A. E., Pettini, M., Dickinson, M., & Giavalisco, M. 2003, *ApJ*, 592, 728
- Steidel, C. C., Shapley, A. E., Pettini, M., Adelberger, K. L., Erb, D. K., Reddy, N. A., & Hunt, M. P. 2004, *ApJ*, 604, 534
- Swinbank, A. M., Chapman, S. C., Smail, I., Lindner, C., Borys, C., Blain, A. W., Ivison, R. J., & Lewis, G. F. 2006, *MNRAS*, 371, 465
- Swinbank, A. M., et al. 2010, *MNRAS*, 405, 234
- Tacconi, L. J., et al. 2008, *ApJ*, 680, 246
- Targett, T. A., Dunlop, J. S., McLure, R. J., et al. 2010, *arXiv:1005.5176*
- Toft, S., Franx, M., van Dokkum, P., Förster Schreiber, N. M., Labbe, I., Wuyts, S., & Marchesini, D. 2009, *ApJ*, 705, 255
- Toft, S., et al. 2007, *ApJ*, 671, 285
- Trujillo, I., Conselice, C. J., Bundy, K., Cooper, M. C., Eisenhardt, P., & Ellis, R. S. 2007, *MNRAS*, 382, 109
- Trujillo, I., et al. 2006a, *MNRAS*, 373, L36
—, 2006b, *ApJ*, 650, 18
- van Dokkum, P. G., et al. 2008a, *ApJ*, 677, L5
—, 2008b, *ApJ*, 677, L5
—, 2010, *ApJ*, 709, 1018
- Williams, R. J., Quadri, R. F., Franx, M., van Dokkum, P., Toft, S., Kriek, M., & Labbé, I. 2010, *ApJ*, 713, 738
- Wirth, G. D., et al. 2004, *AJ*, 127, 3121

Zirm, A. W., et al. 2007, ApJ, 656, 66

